Appl Phys A (2010) 98: 901–908
DOI 10.1007/s00339-009-5474-x

Applied Physics A
Materials Science & Processing

Effect of ambient gas on the expansion dynamics of plasma plume formed by laser blow off of thin film

Sony George · Ajai Kumar · R.K. Singh · V.P.N. Nampoori

Received: 13 August 2009 / Accepted: 20 October 2009 / Published online: 20 November 2009

Abstract A study has been carried out to understand the influence of ambient gases on the dynamics of laser-blow-off plumes of multi-layered LiF–C thin film. Plume images at various time intervals ranging from 100 to 3000 ns have been recorded using an intensified CCD camera. Enhancement in the plume intensity and change in size and shape occurs on introducing ambient gases and these changes are highly dependent on the nature and composition of the ambient gas used. Velocity of the plume was found to be higher in helium ambient whereas intensity enhancement is greater in argon environment. The plume shapes have maximum size at 10^{-2} and 10^{-1} Torr of Ar and He pressures, respectively. As the background pressure increases further ($>10^{-2}$ Torr: depending on the nature of gas), the plume gets compressed/focused in the lateral direction. Internal structure formation and turbulences are observed at higher pressures ($>10^{-1}$ Torr) in both ambient gases.

PACS 52.38.Mf · 52.38.-r

1 Introduction

The laser blow off (LBO) [1, 2] involves the laser beam interaction with thin film supported on a thick transparent substrate, and the ablated material thereby propagates along the direction of incident laser beam. This technique is widely used in trace-element ejection in plasma environment [3], thin film deposition [4] and thin film reflectance studies [5]. Also, the LBO scheme is a powerful technique to produce the neutral atomic beams in the thermal to super-thermal range, which are extensively used in plasma diagnostics for measuring edge plasma parameters and impurity transport in tokamak plasmas [6, 7].

The optical emission spectroscopic technique of LBO plume [8–10] has revealed that expansion feature of plume is highly dependent on the experimental conditions and varies according to the ambient environment and laser fluence. But this technique cannot provide information regarding the influence of experimental parameters on the structure of the plasma plume. The shape and size of the plume in the presence of ambient gas play crucial roles in thin film deposition, formation of nanoparticles & clusters, extreme ultraviolet (EUV) lithography and are important parameters for probing neutral atomic beam in plasma environment. Hence, the understanding of structural formation in the ejected plume species and its spatial and temporal variations with different experimental condition are essential for using these techniques in applied research. Further, the comparative analysis of the plume expansion in vacuum and ambient environment can provide the knowledge of many physical processes, such as deceleration, attenuation/enhancement of emission, hydrodynamic instabilities, formation of shock waves and plume oscillations [8, 11]. It is worth mentioning that neutral species are the main constituents of the LBO plumes although it also consists of the ions mostly in singly ionised state [8]. Hence, it will be worthwhile to study the interaction between background gas and neutral rich plume with regard to the formation of structures in plume due to hydrodynamic instability and reactive scattering.

S. George · V.P.N. Nampoori
ISP, Cochin University of Science and Technology,
Cochin 682 022, India

A. Kumar (✉) · R.K. Singh
Institute For Plasma Research, Gandhinagar 382 428, India
e-mail: ajai@ipr.res.in
e-mail: ajaiipr@yahoo.com
Fax: +91-79-23962277

Recently, we have characterized the expanding LBO plasma plume by imaging overall visible plume emission in Ar ambient using fast photographic technique [12]. This technique has provided the information about the *local* structures, dynamics of the constituent particles and geometrical aspects of the plume at different gas pressures. It has been observed that shape, size and dynamics of the expanding plume are completely modified by introducing the Ar gas. An interesting feature, i.e. a strong confining/focusing effect has been observed in presence of ambient Ar gas. The plume focusing effect has been proposed to be a gas hydrodynamical phenomenon. Therefore, we were motivated to study the effect of different ambient gases. Helium as an ambient environment has been chosen for comparison due to the large difference in its atomic mass and ionisation potential as compared to Ar for having a better understanding of the atomic processes involved during the plume-ambient atom interactions. This experiment can provide information inputs for modelling of the observed plume confinement/focusing.

In the present report, we have studied the evolution features of LBO plume in He and Ar environments with special attention on the comparison of the structure formation in the expanding plume in these two ambient. The enhancement in emission intensity, expansion velocity and validity of different expansion models for He and Ar ambient are also discussed.

2 Experimental setup

A detailed description of experimental setup has been reported in our previous papers [8, 9]. Only the main features and additional part of the setup are summarized here. The experiment has been carried out in a cylindrical stainless steel chamber, which is evacuated to a base pressure better than 2×10^{-5} Torr. Background gas is introduced into the chamber at desired pressures through a fine controlled needle valve. The target is composed of uniform layers of 0.05-μm LiF film and 0.5-μm thick carbon film, deposited on a 1.2-mm thick quartz substrate. The target is mounted on a movable target holder through vacuum compatible feedthrough for fresh film positioning after exposure to the laser beam.

Nd:YAG ($\lambda = 1064$ Å) laser having 8-ns pulse width with maximum pulse energy 1.6 J has been used to ablate the thin film target. The laser beam is focused on the target at an incident angle of 6° with respect to the normal to the surface. The spot size of the laser beam is set to about 1 mm in diameter at the target. By adjusting the operating parameters of laser, laser fluence ranging from 2.8 to 26 J/cm^2 are achieved at the target surface. To ensure that the LBO plume contained only the species of the multi-layered film, the maximum energy density is set below the ablation threshold of the quartz substrate.

The light emitted from the luminous plasma is transmitted though a quartz window mounted orthogonal to the direction of plume expansion. The time-resolved images of the visible plume luminescence have been recorded using an ICCD camera (4 Picos, Stanford Computer Optics, Inc.) having variable gain & gating on time and having a spectral range of 350–750 nm. In the present experiment, the intensifier micro-channel plate (MCP) voltage and gate opening (integration) time is optimised at 900 V and 4 ns, respectively. Temporal evolution of the LBO plume is obtained by varying the time delay (from 100 to 2500 ns) between the laser pulse and opening time of the ICCD gate. Five images are recorded under similar experimental conditions. These images were found to be nearly identical in shape and the reproducibility of the emission intensity is better than 5%. A mesh image of known dimension has been recorded in order to map the geometrical parameters of the plume. The magnification of the imaging system was found to be 3.5. Dark current noise is subtracted from the recorded image using MATLAB. Length and full width at half maximum of the plume were estimated by segmentation algorithm. For better visibility, grey images are converted into pseudo-colour images using jet colour map. A micro-controller-based time control unit is used to trigger the camera in synchronous with the laser pulse. Timing jitter in time delay with respect to laser pulse is less <1 ns.

To measure the spatio-temporal evolution of spectral lines, the plasma plume is viewed normal to the direction of expansion and imaged at the entrance slit of a monochromator ($\Delta\lambda = 12.5$ Å). The temporal profile of emission signal is detected using a photomultiplier tube (PMT) and output of the PMT is directly fed to a 1-GHz digital oscilloscope. A small fraction of the light reflected from the laser-focusing lens is detected by a photodiode and is used as time reference for both oscilloscope and ICCD.

3 Results and discussions

To understand the effect of ambient gas on the shape and dynamics of expanding plume, the temporal evolution of emitting plume driven by the collisional processes between electrons, ions and neutrals is imaged by ICCD camera in He and Ar environments under identical experimental conditions. The sequences of images at different time delays from 400 to 2500 ns and at different gas pressures (varied from 10^{-5} to 3 Torr) are shown in Fig. 1. All the images are recorded at a laser irradiance of $\sim$3 GW cm^{-2} and are normalized to the maximum intensity. Each image represents the spectrally integrated emission intensity in the range of 350–750 nm emitted from different plume species.

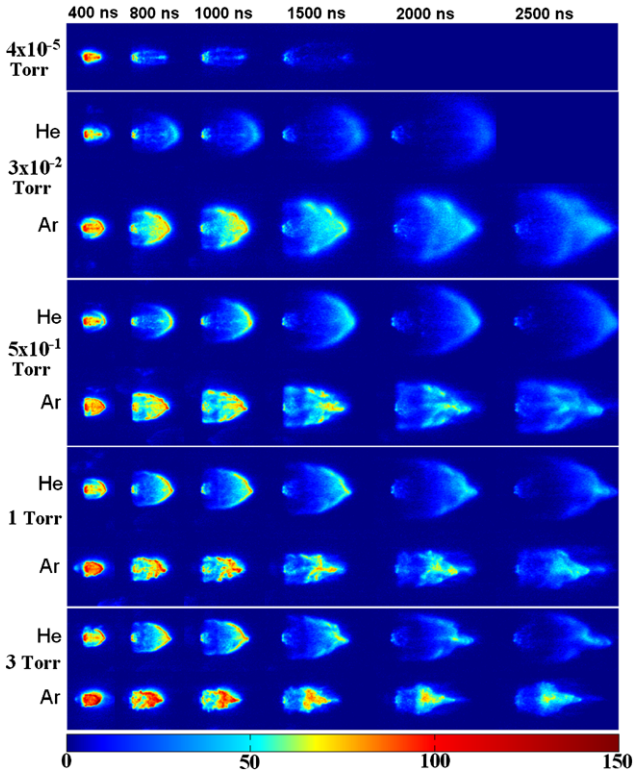

Fig. 1 The sequence of images of expanding plasma plume in He and Ar environment at different time delays. The integration time of ICCD was fixed at 4 ns. The ambient gas pressure was varied from 10^{-5} to 3 Torr. *Colour bar* shows the normalised intensity in arbitrary unit

Focused laser beam strikes on the LiF–C film and the generated plasma plume expands in the forward direction under the influence of pressure gradient. In vacuum, the plume expands adiabatically and has an ellipsoidal shape. It shows a non-uniform intensity pattern parallel to the direction of plume expansion and is more intense at the leading edge of the plume and at points closer to the target. During expansion, the electron density reduces rapidly and hence the probability of electron impact excitation is also reduced. This leads to considerable reduction in the emission intensity of the plume. For $t > 1000$ ns, emission intensity is beyond the detection limit of the ICCD because of the relatively low dynamic range of the camera.

The shape, size and emission intensity are highly dependent on the nature of the ambient gas. Careful examination of plume images at intermediate pressure regime of He (10^{-2} Torr) indicates that the major portion of the shape and size of the plume is nearly identical to that observed in vacuum (up to 1500 ns) except the plume front. A luminous wake-like structure, wider than the plume size in vacuum, is formed at the plume front in presence of He gas. These images are significantly different as compared to the observed images in 10^{-2} Torr of Ar environment. The emission intensity and lateral expansion of the plume is more prominent in Ar environment than in He environment. For a fixed time delay, plume generated in He ambient propagates longer distance than in Ar gas (Fig. 1). In 10^{-2} Torr of He, front end of the plume remains unchanged up to a time period of 2 μs after the plasma formation. On the other hand, there is a strong lateral focusing, which starts after ∼1 μs in 10^{-2} Torr Ar environment. The above observations indicate that the nature of the ambient gas, e.g. atomic mass, ionisation energy and thermal conductivity, greatly influence the expansion dynamics of LBO plume.

At 10^{-2} Torr pressure and time delay $t > 400$ ns, the plume expands in the collisional regime where the estimated plume dimension (∼7 mm) is greater than the mean free path of the ejected species [8]. In this regime, interpenetration of the plasma plume into the ambient gas occurs, which causes an increase in collisions between the plume species and ambient gas atoms. The increase in collision processes is responsible for the enhancement in the observed emission intensity. With increasing time delay, plume becomes more collisional and at $t > 2500$ ns, plume species diffuse into the background gas. Due to the smaller mass of He, higher diffusion into the plume is expected in comparison to Ar, but we could not see any significant enhancement in emission intensity in He especially inside the plume in this pressure regime.

It is worth mentioning here that carbon atoms (major constituents in the plume) change its direction by ∼15 and ∼78° in collision with He and Ar atom, respectively [13]. Therefore in the collisional regime, divergence of plume species increases with the mass of the background atoms, which is in agreement with observed plume width (larger in Ar environment as compared to He up to the 1500 ns and at 10^{-2} Torr pressure). However at 2000 ns, the size of plume in He is bigger than the observed size in Ar. This is because in this regime, the confining effect (discussed later) might be starting to dominate over the scattering processes.

In conventional laser-produced plasma (LPP) experiment, Kedreja et al. [14] studied the line emission intensity of carbon in He and Ar environment and found that higher emission occurred in He environment. They suggested that the probable mechanism responsible for the increase in emission intensity should be the plasma confinement produced by the background gas, resulting in increase in emission. Similar conclusion has also given by Gonjalo et al. [15] on comparing the line emission intensity in oxygen and Ar environment.

In our case, we observe large enhancement in emission at 10^{-2} Torr of Ar pressure and could not see any signature of plume confinement as compared to the observed images in vacuum. The above observation is supported by our optical emission spectroscopy data recorded in identical experimental conditions. Figure 2 shows the time and space resolved emission profiles for Li I (at 670.8 nm) lines in vacuum and different pressures of He and Ar and at a distance

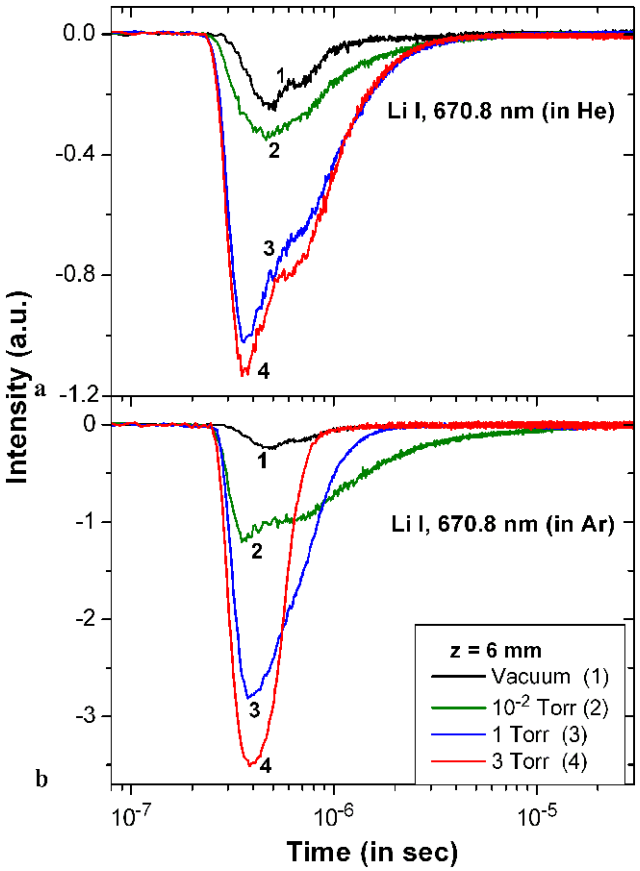

Fig. 2 Temporal evolution of Li I (at 670.8 nm) emission lines for different (**a**) He and (**b**) Ar gas pressures. The profiles were recorded at distance 6 mm from the target

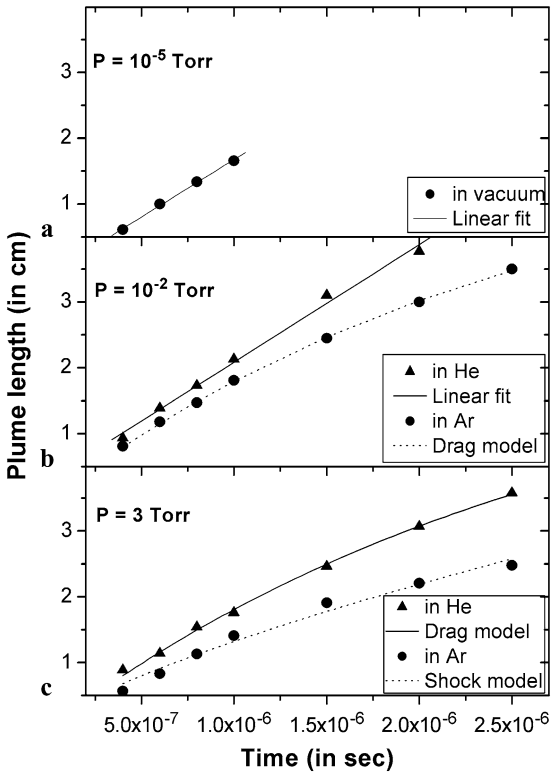

Fig. 3 Observed plume length as a function of time delay for three different ambient environments (**a**) vacuum, (**b**) 10^{-2} Torr and (**c**) 3 Torr of He and Ar pressure. The *solid* and *dashed lines* represent the best fit of the experimental data with appropriate models

of 6 mm away from the target. With increase in He pressure from vacuum to 1 Torr, the emission intensity increased with pressure. Almost similar intensity is observed at 1 and 3 Torr pressure. However, the emission intensity is enhanced drastically at 10^{-2} Torr of Ar pressure as compared to the observed intensity in vacuum. At this pressure, the total intensity (integrated area under the curve) is enhanced by a factor of ∼2.6 and ∼15 in He and Ar environments respectively. At relatively higher Ar pressures (1 & 3 Torr), there is a sharp increase in peak intensity. The integrated emission intensity is nearly equal for 10^{-2}, 1 and 3 Torr of Ar pressure. Moreover, we do not observe any confining effect at 10^{-2} Torr of Ar or in the entire pressure regime of He. It is worthwhile to mention that the spectroscopic measurements predict only the longitudinal confinement, and they are unable to provide information regarding the lateral confinement. The above observations suggest that the confinement mechanism alone is not adequate enough to explain the enhancement in overall emission intensity and therefore some other processes are possibly responsible for the observed results.

In the present case, the increase in emission intensity of the expanding plume in background gas can be attributed mainly to two processes: (1) excitation due to collisions with background atoms and (2) electron impact excitation/recombination. Between these two cases, electron impact processes should play a dominant role in excitation, as the cross-sections of atom–atom collision are two orders of magnitude lower than the electron–atom collisions [16]. The interaction between the expanding plume front and ambient gas can cause the ionisation of ambient gas, which contributes to the increase in electron density. The transfer of kinetic energy from the plume front to the background gas via ion–ion Coulomb scattering, ion–neutral collisions, charge exchange interactions, etc. is clearly observed at low-pressure regime of He. Since the ionisation energy of He is greater than Ar, more increase in electron density is expected in Ar environment. Another factor, which can be accounted for the large difference in the emission intensity in He and Ar environments is cascade growth of the electron number density and absorption coefficient of the plasma in ambient environment [17, 18]. The condition for the cascade growth is expressed as

$$\frac{d\varepsilon}{dt} = \frac{4\pi^2 e^2 I \nu_{\text{eff}}}{m_e c \omega^2} - \frac{2 m_e \nu_{\text{eff}} E}{M} > 0 \qquad (1)$$

where ε is the electron energy; e and m are the charge and the mass of an electron; M is the mass of the background

gas; E is the ionisation energy of the gas; υ_{eff} is the effective frequency of electron–neutral collision; I is the radiation intensity; and ω the frequency of the radiation. On comparing the atomic data of He and Ar, the condition for cascade growth is more favourable in Ar environment than He. This indicates that electron temperature and density of the plasma plume should be higher in Ar ambient as compared to He [18, 19]. This will result in increase in electron impact excitation, which is largely dependent on electron temperature and density. Of course, this is reflected in our results, where the emission intensity in Ar is higher as compared to He environment.

Further, the rate of change of electron temperature in the plasma is the sum of three terms viz., elastic collision, electron heating due to collisional de-excitation of metastable ions and recombination of ions. The rate of loss of electron energy at short times is mainly dominated by the elastic collision term $Q_{\Delta t}$, which is inversely proportional to mass of background gas and hence lighter gases are efficient for rapid cooling. Helium, being the lighter gas compared to Ar, gives rise to rapid cooling. Also, due to the higher thermal conductivity of He, plume generated in He cools very fast as compared to that in Ar. The decrease in electron temperature directly influences the collisional processes inside the plume resulting in the reduction in emission intensity in He ambient.

As the background pressure is further increased to 3×10^{-1} Torr, the plume appears compressed along the lateral direction in Ar ambient as compared to the observed plume size at 10^{-2} Torr whereas in case of He, we did not see any lateral confinement in the plume, though the width of the plume further increased at 3×10^{-1} Torr pressure. In He, the lateral confinement starts at a later stage of the plume expansion at 1 Torr pressure. On comparing the plume expansion at fixed time delay and pressure $>3 \times 10^{-1}$ Torr, it is observed that the longitudinal and lateral dimension of the plume is higher in He environment in comparison to Ar. This is expected, because the higher mass of the ambient atoms leads to better confinement. At this pressure, interpenetration of the plume species and background gas is relatively weak [8, 11]. The plume material pushes more against the ambient gas, which results in the formation of a layer of compressed gas around the plume as sharp boundary.

It should be noted that, the cascade growth should not be favoured at this pressure regime because of the increased energy loss due to elastic collision of the electrons with the neutral particles of the gas. However at this pressure, greater confinement of the plasma can take place, which can enhance the frequency of elastic and inelastic collisions and thereby increase the probability of excitation. This effect can be traced from Fig. 1, where the confined images in Ar ($>10^{-2}$ Torr pressure) are more intense than in He.

It is important to see that the effect of background gas is more pronounced in the lateral direction than in the direction of expansion as is evident from the images at 10^{-1} Torr of Ar and 3 Torr of He (Fig. 1). A narrow stream of dense emission is observed along the centre-line of the plume, which propagates like free expansion in vacuum. This can be explained in terms of sequence of formation of LBO plume. The energetic species produced by direct laser ablation (mostly the ions) form the leading edge of the plume. On the other hand, the remaining material is propelled from the substrate in the form of neutral vapour, moving with much lower translational energy as compared to the energetic front. Due to the higher translation energy, energetic front penetrates into the ambient gas with little interaction and therefore, has same velocity as in vacuum. On the other hand, the slow component of the plume undergoes gas hydrodynamic effect resulting in nonlinear expansion in ambient environment.

As mentioned earlier, a sharp and intense contact boundary is formed at the interface between the plasma and ambient gas. It is observed that disturbances on the contact boundary (edge turbulence) appeared with increasing the pressure. This effect is clearly noticed for pressures $>10^{-1}$ Torr of Ar and >1 Torr of He. The hydrodynamical instability (e.g. R–T instability) is one of reason to produce the turbulence at the edge region. The critical density required to produce the R–T instability [8] is given by, $\rho_b = 3m/4\pi R^3$; where m is the mass of ablated material and R is the plume dimension. Considering the mass of the ablated material as 0.992 μg [8] and the measured plume length ~7.3 mm (at 400 ns). The estimated background gas density required for R–T instability comes out to be 0.609 μg/cm^3, which corresponds to a pressure of ~3 Torr for He and $\sim 3 \times 10^{-1}$ Torr for Ar. This is in agreement with the observed edge turbulence in He and Ar environment.

Apart from the edge turbulence, the interaction of the expanding plume with the background atoms also affects the central part of the plume. The breaking of plume images is clearly observed for the pressure $\geq 10^{-1}$ Torr of Ar. Though we did not observe any significant change in the internal structure in He background, some distortion inside the plume however, appeared at 1500-ns time delay and 3-Torr pressure. This might be due to the fact that at higher background pressures (depending on mass of the gas), the ambient gas penetrates into the plume, which could lead to collisions inside the plume. As a result, generation of complex internal structural patterns can take place inside the plume.

Another important observation during the expansion of plume in the ambient environment is the focusing/narrowing of the LBO plume in the lateral direction. The strength of the focusing is found to be dependent on the time delay as well as nature and pressure of the ambient gas. In Ar ambient, the focusing effect starts after 1000 ns at 10^{-1} Torr

pressure and it persists for 3.5 μs time delay without any noticeable divergence. This effect is observed up to pressure of 3 Torr. Similar phenomenon is also observed in He at 3 Torr pressure and for time delay >1000 ns. Due to limitations of our experimental setup, we could not exceed the ambient pressures greater than 3 Torr in He in order to confirm the focusing strength and divergence of plume in He.

In our previous spectroscopic studies of LBO plume [8, 10], it has been established that for these range of pressures and time delays, most of the emission comes from the neutral species. Images have also been recorded with an interference filter (corresponding to the neutral lithium line: centre wavelength 670.8 nm, FWHM ∼ 1 nm) fitted in front of ICCD camera for both the ambient gases. Appearance of similar pattern in recorded images, with and without filter suggests that plume focusing is, of course, a gas hydrodynamic phenomenon.

Similar focussing/narrowing of the plasma plume in presence of ambient gas has been reported for conventional LPP experiments under different experimental schemes [20–22]. Bulgakova et al. [22] proposed a most realistic model to explain the focusing (lateral confinement) of laser-produced plasma based on the analogy between an ablated plume and a supersonic under-expanded gaseous jet expanding into the background gas. This model predicts the strength of focusing dependent on the mass of the background atoms and it occurs over a short spatial region and thereafter diverges out. Again with increasing ambient gas pressure, the focusing effect becomes more pronounced and the point of focus shifts towards the target. We have observed the focusing of the plume in both Ar and He, which exhibits dependence on the mass of ambient gas. However, we could not notice any divergence of plume after focusing or shift of focus position of the plume towards target with increasing the ambient pressure. Therefore, we feel that more theoretical and experimental investigations may be required to explain the present plume-focusing phenomenon in terms of gas hydrodynamics and atomic physics associated with it.

As discussed earlier, expansion of the plume shows the characteristic dependence on the nature of the ambient gas and its pressure regime. To illustrate the plume propagation in different pressure regimes, we have estimated the plume length (corresponds to distance travelled by the plume) versus time and the observed results are interpreted with appropriate models. A linear dependence of the plume length with time in vacuum suggests free expansion of plasma plume (Fig. 3a). At 10^{-2} Torr of He pressure, the plume propagation is almost independent of the ambient pressure and follows vacuum-like expansion (Fig. 3b). In case of 10^{-2} Torr of Ar, plume expands freely up to 1000 ns and thereafter it tends to slow down, as it experiences a viscous drag force exerted by the heavier Ar atoms. The slowing down of ejected species is well fitted with the classical drag force model [23], $z = z_f[1 - \exp(-\beta t)]$ where β is the slowing coefficient and z_f is the stopping distance of the plume. The best fitting parameters give a slowing coefficient β equal to 3.8×10^5/s and stopping distance equal to 5.6 cm. The plume expansion in 3 Torr of He pressure follows similar behaviour as observed in 10^{-2} Torr of Ar (Fig. 3c). It also follows the drag force model and the fit parameters are $\beta = 3.5 \times 10^5$/s and $z_f = 6.05$ cm. On the other hand, at relatively high pressures (3 Torr) of Ar, a shock wave [24] starts even at 400 ns time delay as the mass of the Ar gas becomes comparable to the mass of the ablated species [6]. In this region, $z \propto t^{0.72}$ dependence of plume propagation is in close agreement with the shock model (Fig. 3c).

We have also compared the measured plume length in different gas pressure using the adiabatic expansion model [25]. According to this model, plume expansion is stopped as the plasma pressure approaches the ambient gas pressure. The stopping distance (and therefore the plume length) is then given by

$$L = A\left[(\gamma - 1)E\right]^{1/3\gamma} P^{-1/3\gamma} V_i^{(\gamma-1)/3\gamma} \tag{2}$$

where γ is the specific heat ratio, E is the laser energy, P is the ambient pressure and V_i is the initial volume of the plume at the end of the laser pulse. A is the geometrical factor, which depends on the expansion angle θ for a conical plume,

$$A = (1 + 1/\tan\theta)\left[3\tan\theta/(\pi + 2\pi\tan\theta)\right] \tag{3}$$

Taking $\gamma = 1.66$, $E = 200$ mJ, $\theta = 30°$ and $V_i = 4.61 \times 10^{-4}$ cm^3 (taking initial plume velocity of 7.35×10^6 cm/s and the laser spot and pulse duration 1 mm and 8 ns respectively), the calculated plume length using relation (2) is shown in Fig. 4. The measured plume length at different gas pressures of Ar after 3000 ns of plume initiation are also included in Fig. 4. It should be noted that the measured plume length at 3000 ns is not the stopping distance as the plume may further expand with increasing the time delay. This conclusion is inferred from the fitting parameters of the drag force model that gives the stopping distance of 56 mm for the plume expansion in 10^{-2} Torr of Ar. It should be pointed out that, the observed plume length cannot be compared directly with the calculated plume length. However, the trend of decreasing plume length with ambient gas pressure can be noticed clearly. The LBO plume does not follow the adiabatic expansion model as the plume propagates longer distances as compared to the predicted distance by it. This may arise due to the formation of energetic plume front in LBO, which penetrates the ambient gas without much attenuation in temperature and hence similar expansion velocity.

To understand the lateral confinement of plume, the variation in plume width as a function of time as well as gas pressures of He and Ar, are presented in Fig. 5. It is observed

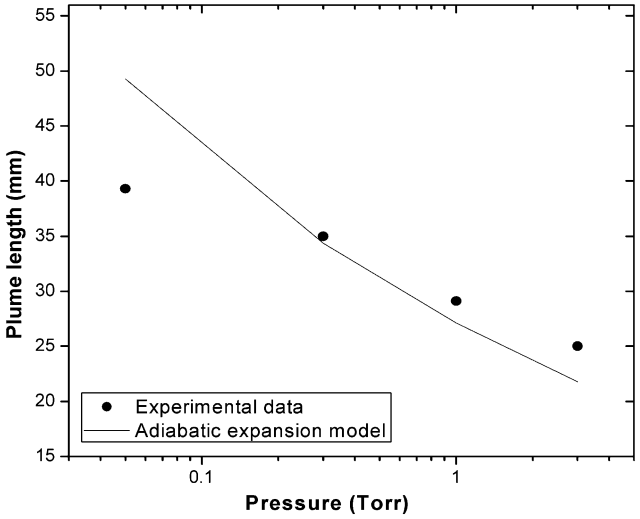

Fig. 4 Observed plume length at 3000-ns time delay for different Ar gas pressures. *Solid line* represents the estimated plume length using the adiabatic expansion model

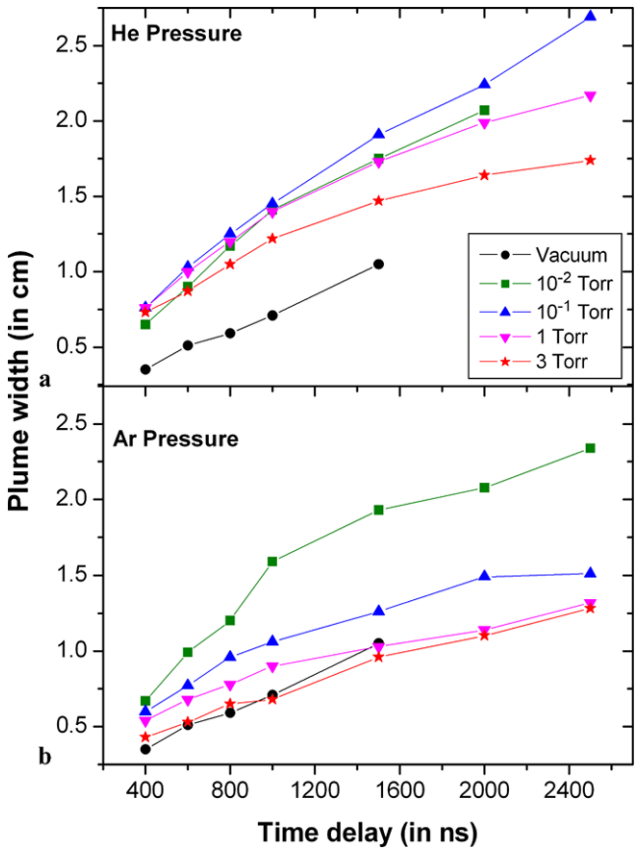

Fig. 5 Variation of plume width with time delay in different pressure regime of (**a**) He and (**b**) Ar gas

that up to 10^{-1} Torr of He pressure, width of the plume increases with time. With further increase in the pressure up to 3 Torr, the plume confinement starts after a time delay of 1000 ns (width of the plume gradually decreases with

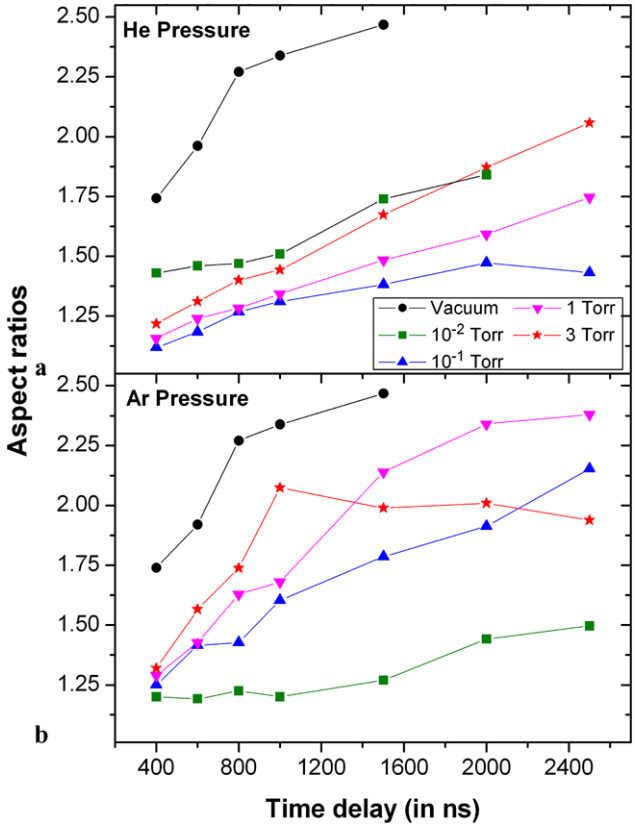

Fig. 6 Aspect ratio (length/width) of the plume as a function of time delay for different gas pressures of (**a**) He and (**b**) Ar

increasing the pressure), whereas in case of Ar, the maximum width was observed at 10^{-2} Torr and it starts reducing (confining/focusing) with further increase in pressure. The comparison of the plume width in He and Ar reveals that plume width reduces more in Ar than in He. At 2500 ns, the width of the plume at 3 Torr reduces to half of the width observed at 10^{-2} Torr of Ar pressure. To illustrate the effect of the ambient environment on the two-dimensional shape of the plume, the aspect ratio (length/width) as a function of time delay is plotted (Fig. 6). For both He and Ar ambient, it has been found that the aspect ratio increases with pressure for fixed time delay, because there is reduction of width with pressure without any appreciable change in length of the plume. However, some differences between the He and Ar ambient are observed especially, at 10^{-2} Torr and 3 Torr pressure. In Ar, plasma plume is nearly hemispherical (width $\sim$ length) up to the 1000 ns for the gas pressure 10^{-2} Torr. The aspect ratios comes close to the saturation for $t \geq 1000$ ns at 3 Torr Ar pressure; which indicates that this pressure restricts the lateral as well as forward motion of the plume species in the same proportion. However, these effects are not observed in He environment.

4 Summary

We report the study of the expansion dynamics of laser-blow-off (LBO) plasma plume under the influence of He and Ar ambient pressures using fast imaging technique. It has been observed that a plume expands adiabatically in vacuum and has an ellipsoidal shape. Enhancement in the plume luminosity and change in size & shape occurs on introduction of ambient gases and these changes are highly dependent on the nature and composition of the background gas used. Velocity of the plume front has been found to be higher in He ambient whereas intensity enhancement is greater in Ar environment. The plume shapes have maximum size at 10^{-2} and 10^{-1} Torr of Ar and He pressure, respectively. With further increase in the background pressure, a high luminescent boundary forms between ambient gas and the plume gets compressed and focused in the lateral direction. This effect is more pronounced in Ar environment as compared to He. It is found that R–T instability is responsible for the turbulence on the edge region of the plasma plume. At higher ambient gas pressures (depending on the nature of the gas), structures are developed inside the plasma plume due to hydrodynamic instability. From the R/t plots, it is found that at earlier stages (<1000 ns) the expansion is almost linear irrespective of the background gas pressure. Later on velocity plot deviates from linearity due to interaction between the plume and ambient gas. In vacuum, plasma plume follows the linear expansion whereas in the presence of ambient gas it follows drag force and shock wave models depending on the nature and pressure of the gas.

Acknowledgements Sony George acknowledges UGC for research fellowship (RFSMS) and also IPR for support and permission given to pursue this work. Authors thank Dr. H.C. Joshi, Dr. Ravi A.V. Kumar for critical evaluation of manuscript and Mr. Vishnu Chaudhari and Mr. Kiran Patel for their technical help.

References

1. F.J. Adrian, J. Bohandy, B.F. Kim, A.N. Jette, P. Thomson, J. Vac. Sci. Technol. B **5**, 1490 (1987)
2. V. Schultze, M. Wagnev, Appl. Phys. A **53**, 241 (1991)
3. R. Koppmann, S.M. Refaei, A. Pospieszczyk, J. Vac. Sci. Technol. A **4**, 79 (1986)
4. J. Bohandy, B.F. Kim, F.J. Adrian, J. Appl. Phys. **60**, 1538 (1986)
5. A.B. Bullock, P.R. Bolton, F.J. Mayer, J. Appl. Phys. **82**, 1828 (1997)
6. A. Pospieszczyk, F. Aumayr, E. Hintz, B. Schweer, J. Nucl. Mater. **162–164**, 574 (1989)
7. T. Parisot, R. Guirletl, C. Bourdelle, X. Garbet, N. Dubuit, F. Imbeaux, P.R. Thomas, Plasma Phys. Control. Fusion **50**, 055010 (2008)
8. R.K. Singh, A. Kumar, B.G. Patel, K.P. Subramanian, J. Appl. Phys. **101**, 103301 (2007)
9. A. Kumar, R.K. Singh, K.P. Subramanian, B.G. Patel, S. Sunil, I.A. Prajapati, J. Phys. D, Appl. Phys. **39**, 4860 (2006)
10. A. Kumar, R.K. Singh, V. Prahlad, H.C. Joshi, J. Appl. Phys. **104**, 093302 (2008)
11. S. Amoruso, B. Toftmann, J. Schou, R. Velotta, X. Wang, Thin Solid Films **453–454**, 562 (2004)
12. S. George, A. Kumar, R.K. Singh, V.P.N. Nampoori, Appl. Phys. Lett. **94**, 141501 (2009)
13. W.D. Westwood, J. Vac. Sci. Technol. **15**, 1 (1978)
14. T. Kerdja, S. Abdelli, D. Ghobrini, S. Malek, J. Appl. Phys. **80**, 5365 (1996)
15. J. Gonzalo, F. Vega, C.N. Afonso, J. Appl. Phys. **77**, 6588 (1995)
16. C. Timmer, S.K. Srivastava, T.E. Hall, A. Fucaloro, J. Appl. Phys. **70**, 1888 (1991)
17. Y. Iida, Spectrochim. Acta B **45**, 1353 (1990)
18. S.S. Harilal, C.V. Bindhu, V.P.N. Nampoori, C.P.G. Vallabhan, Appl. Phys. Lett. **72**, 167 (1998)
19. J.A. Aguilera, C. Aragon, Appl. Phys. A **69**, S475–S478 (1999)
20. X.K. Shen, J. Dun, H. Ling, Y.F. Lua, Appl. Phys. Lett. **91**, 081501 (2007)
21. D.J. Lichtenwalner, O. Auciello, R. Dat, A.I. Kingon, J. Appl. Phys. **74**, 7497 (1993)
22. A.V. Bulgakov, N.M. Bulgakova, J. Phys. D, Appl. Phys. **31**, 693 (1998)
23. J.C.S. Kools, J. Appl. Phys. **74**, 6401 (1993)
24. W.K.A. Kumuduni, Y. Nakayama, Y. Nakata, T. Okada, M. Meada, J. Appl. Phys. **74**, 7510 (1993)
25. P.E. Dyer, A. Issa, P.H. Key, Appl. Phys. Lett. **57**, 186 (1990)